HHS Public Access

Author manuscript

Eur J Pharmacol. Author manuscript; available in PMC 2019 February 05.

Published in final edited form as:

Eur J Pharmacol. 2018 February 05; 820: 8–17. doi:10.1016/j.ejphar.2017.12.006.

Synthesis and *in vitro* characterization of a P2X7 radioligand [^{123}I]TZ6019 and its response to neuroinflammation in a mouse model of Alzheimer Disease

Hongjun Jin[1,5], **Junbin Han**[1], **Derek Resing**[1], **Hui Liu**[1], **Xuyi Yue**[1], **Rebecca L. Miller**[2], **Kathleen M. Schoch**[2], **Timothy M. Miller**[2], **Joel S. Perlmutter**[1,2,3], **Terrance M. Egan**[4], and **Zhude Tu**[1,*]

[1]Department of Radiology, Washington University School of Medicine, St. Louis, MO 63110, USA

[2]Department of Neurology, Washington University School of Medicine, St. Louis, MO 63110, USA

[3]Department of Neuroscience, Physical Therapy and Occupational Therapy, Washington University School of Medicine, St. Louis, MO 63110, USA

[4]Department of Pharmacological and Physiological Science, Saint Louis University School of Medicine, St. Louis, MO 63104, USA

Abstract

The purinergic receptor P2X ligand-gated ion channel 7 (P2X7 receptor) is a promising imaging target to detect neuroinflammation. Herein, we report development of a potent iodinated labeled radiotracer for P2X7 receptor, [^{123}I]TZ6019. The radiosynthesis of [^{123}I]TZ6019 was accomplished by allylic-tin precursor iodination using [^{123}I]NaI with good radiochemical yield of 85% and high radiochemical purity of > 99%. Human embryonic kidney 293 (HEK-293) cell line stably transfected with the human P2X7 receptor was used to characterize the binding affinity of TZ6019 in fluorescence, radioactive competitive, and saturation binding assays. A radioligand competitive assay with [^{123}I]TZ6019 demonstrated that the nonradioactive compound TZ6019 has an IC_{50} value of 9.49 ± 1.4 nM, and the known P2X7 receptor compound GSK1482160 has an IC_{50} value of 4.30 ± 0.86 nM, consistent with previous reports. The radioligand saturation binding assay and competitive assay revealed that [^{123}I]TZ6019 specifically bound to the human P2X7 receptor with high affinity (K_i = 6.3 ± 0.9 nM). *In vitro* autoradiography quantification with brain slices collected from 9-month old P301S tau transgenic mice along with wild type controls, revealed higher binding of [^{123}I]TZ6019 (35% increase) in the brain of P301S transgenic mice (n = 3, p = 0.04) compared to wild type controls. The immunofluorescence microscopy confirmed that expression of P2X7 receptor was colocalized with astrocytes in the tauopathy P301S

*Corresponding Author, Tel.: +1-314-362-8487; Fax: +1-314-362-8555; tuz@mir.wustl.edu.

[5]Current address: Research Center of Molecular Imaging, Sun Yat-sen University Fifth Affiliated Hospital, Zhuhai City, Guangdong Province, China 519000

Disclosure

The authors do not have any conflict of interest.

transgenic mice. [^{123}I]TZ6019 has specific binding for P2X7 receptor and has great potential to be a radiotracer for screening new compounds and quantifying expression of P2X7 receptor in neuroinflammation related diseases.

Keywords

Neuroinflammation; P2X7 receptor; P301S; I-123

1. Introduction

Neuroinflammation plays an important role in progression of many neurodegenerative diseases including Alzheimer disease (AD) and Parkinson disease (PD) (Bhattacharya and Biber, 2016; Monif et al., 2010). Elevated purinergic receptors expression has shown close association with neuroinflammation due to the large release of adenosine/uridine derivatives from the damage site (Bhattacharya et al., 2013; Boumechache et al., 2009). Purinergic receptors are adenosine-triphosphate (ATP) gated non-selective ion channels which are expressed on the surface of many different cell types (Able et al., 2011; Burnstock, 2009a, b). Among these purinergic receptors, P2X7 receptor has been implicated in microglial activation, astrogliosis, or phagocytosis at sites of injury (Bartlett et al., 2014; Bhattacharya and Biber, 2016; Franke and Illes, 2014; Grygorowicz et al., 2016), and release of pro-inflammatory cytokines (Bianco et al., 2006; Collo et al., 1997; Ferrari et al., 2006). Upregulation of extracellular ATP in neuroinflammatory conditions significantly increases expression of P2X7 receptor. The P2X7 receptor knockout mice display a significantly reduced neuroinflammatory response (Basso et al., 2009; Monif et al., 2009). Therefore, P2X7 receptor represents a novel molecular target for imaging neuroinflammation. A potent P2X7 receptor antagonist, GSK1482160, has recently been labeled with carbon-11 (half-life 20.4 min) for positron emission tomography (PET) imaging of neuroinflammation in an animal model (Gao et al., 2015; Han et al., 2017; Ory et al., 2016). However, this radioligand showed tight binding to human P2X7 receptor, but weak binding to rodents P2X7 receptor (Gao et al., 2015; Ory et al., 2016). And the human applications of this tracer remain to be explored. New potent ligands specifically targeting both human and rodent P2X7 receptor, and capable to be translated for clinic are still demanding. Screening new analogues for P2X7 ligand development requires a reliable assay platform for P2X7 receptor. For the *in vitro* assays, labeled probes with longer half-life radioisotopes facilitate implementation of these assays. Previously two tritium labeled ligands ([^{3}H]A804598 and [^{3}H]JNJ54232334) have been reported for P2X7 receptor (Donnelly-Roberts et al., 2009; Lord et al., 2015), but they have limited availability. Herein we report the radiosynthesis of the Iodine-123 (half-life 13.3 h) labeled radiotracer [^{123}I]TZ6019 and initial characterization of [^{123}I]TZ6019 for P2X7 receptor. The radiosynthesis of [^{123}I]TZ6019 was accomplished by allylic-tin precursor iodination. The binding properties of [^{123}I]TZ6019 were determined using P2X7 receptor expressed HEK-293 living cells, and *in vitro* autoradiography studies with [^{123}I]TZ6019 were performed with postmortem brain tissue from P301S transgenic mice, a tauopathy mouse model. Our results showed that [^{123}I]TZ6019 is a potent and specific radiotracer for P2X7 receptor, and the binding of P2X7 receptor was associated with the neuroinflammation in the tauopathy mouse model.

2. Materials and Methods

2.1 Chemistry

The structures of several known P2X7 receptor radioligands including [^{123}I]TZ6019 are summarized in Fig. 1. Compound GSK1482160 was synthesized by following the reported procedure (Gao et al., 2015; Han et al., 2017). The standard compound **5** (TZ6019) was also synthesized from demethyl-GSK1482160, depicted in Scheme 1A. All reagents and chemicals were obtained from standard commercial sources and used without further purification, unless otherwise stated. The organic reaction was carried out under inert nitrogen and moisture-free conditions with a dry solvent. Thin layer chromatography (TLC) was used to monitor the reaction with pre-coated glass plates of silica gel 60 F_{254} from EMD Chemicals Inc. (Gibbstown, NJ). The product of each step was purified by silica gel 40–63 μm from SiliCycle Inc. (Quebec City, Quebec, Canada). ^{1}H and ^{13}C spectra were recorded at 400 MHz on a Varian Mercury-VX spectrometer with $CDCl_3$ as solvents and tetramethylsilane (TMS) as the internal standard. The chemical shifts were reported in δ (ppm) values relative to $CHCl_3$ (δ 7.26 ppm for ^{1}H NMR and δ 77.2 ppm for ^{13}C NMR), multiplicities were indicated by s (singlet), d (doublet), t (triplet), q (quartet), m (multiplet), and br (broad). High resolution mass spectrum (HRMS) was performed on a Waters ZQ 4000 single quadrupole mass spectrometer equipped with an electrospray ionization (ESI) LC−MS interface.

2.1.1 (E)-N-(2-chloro-3-(trifluoromethyl)benzyl)-5-oxo-1-(3-(tributylstannyl)allyl)pyrrolidine-2-carbox-amide (4)—At 0 °C, 3 ml Lithium bis(trimethylsilyl)amide (LiHMDS, 1 M in tetrahydrofuran, THF) was added into an oven-dried 100 ml round bottle flask with a solution of compound **3** (600 mg, 1.8 mmol, 1.0 equiv.) in 10 ml dimethylformamide (DMF) (Gao et al., 2015; Han et al., 2017). Then 2.0 equiv. of tributyl-(3-chloro-propenyl)-stannane was added into the flask at 0 °C. The mixture was stirred overnight at room temperature, then extracted with ethyl acetate (EtOAc). The organic solution was dried using Mg_2SO_4, filtered, and concentrated under reduced pressure. The crude product was purified by silica gel column using hexane/EtOAc (1/1, v/v) to yield product **4** as a yellow solid (320 mg, 27% yield). ^{1}H NMR (400 MHz,$CDCl_3$): δ 7.66 (d, J = 7.9 Hz, 1H), 7.57 (d, J = 7.5 Hz, 1H), 7.35 (t, J = 7.8 Hz, 1H), 6.41 (t, J = 5.5 Hz, 1H), 6.02 (d, J = 19.0 Hz, 1H), 5.67 – 5.79 (m, 1H), 4.58 (d, J = 6.0 Hz, 2H), 4.48 – 4.56 (m, 1H), 4.03 (dd, J = 8.8, 3.4 Hz, 1H), 3.26 (dd, J = 15.3, 7.3 Hz, 1H), 2.44 – 2.56 (m, 1H), 2.24 – 2.42 (m, 2H), 1.99 – 2.11 (m, 1H), 1.36 – 1.54 (m, 6H), 1.20 – 1.32 (m, 6H), 0.77 – 0.94 (m, 15H); ^{13}C NMR (100 MHz, $CDCl_3$): δ 175.5, 171.5, 140.5, 137.5, 134.1, 133.8, 131.6, 129.2 (q, J_{C-F} = 28.0 Hz), 127.2 (q, J_{C-F} = 5.4 Hz), 126.9, 122.7 (q, J_{C-F} = 272 Hz), 60.5, 47.6, 41.7, 29.65, 29.0 (J_{C-Sn} = 20.7 Hz), 29.6, 27.2 (J_{C-Sn} = 54.7 Hz), 23.5, 13.7, 9.4 (J_{C-Sn} = 345 Hz). HRMS (ESI) calculated for $C_{28}H_{42}ClF_3N_2O_2Sn$ $[M + H]^+$ 651.1982 revealed $[M + H]^+$ 651.1978.

2.1.2 (S,E)-N-(2-chloro-3-(trifluoromethyl)benzyl)-1-(3-iodoallyl)-5-oxopyrrolidine-2-carboxamide (5)—A solution of iodine in chloroform (0.1 M, 2 ml) was added dropwise to a solution of **4** (130 mg, 0.2 mmol) in dry chloroform (10 ml). The reaction was stirred at room temperature for 20 h. The solution then was diluted with

chloroform (15 ml), washed with saturated $Na_2S_2O_3$ (6 × 25 ml) and then saturated aqueous NaCl solution. The combination of organic layers were dried over anhydrous sodium sulfate, concentrated under reduced pressure. The residue was purified by flash silica gel chromatography using hexane/EtOAc (1/4, v/v) as the eluent to yield the final product **5** (TZ6019) in a brown solid (86 mg, 88% yield). ^{1}H NMR (400 MHz, $CDCl_3$): δ 7.62 (d, J = 7.7 Hz, 1H), 7.53 (d, J = 7.5 Hz, 1H), 7.32 (t, J = 7.8 Hz, 1H), 6.67 (t, J = 5.5 Hz, 1H), 6.42 – 6.24 (m, 1H), 6.18 (d, J = 14.7 Hz, 1H), 4.64 – 4.44 (m, 2H), 4.14 (dd, J = 14.9, 5.2 Hz, 1H), 3.99 (dd, J = 8.5, 3.6 Hz, 1H), 3.31 (dd, J = 15.3, 7.9 Hz, 1H), 2.55 – 2.35 (m, 1H), 2.33 – 2.18 (m, 2H), 1.92 – 2.06 (m, 1H); ^{13}C NMR (100 MHz, $CDCl_3$): δ 175.4, 171.1, 139.2, 137.5, 133.9 (q, J_{C-F} = 1.6 Hz), 129.2 (q, J_{C-F} = 32 Hz), 127.3 (q, J_{C-F} = 5.4 Hz), 127.0, 122.7 (q, J_{C-F} = 272 Hz), 80.6, 60.7, 46.0, 41.8, 29.5, 23.5. HRMS (ESI) calcd for $C1_6H_{15}ClF_3IN_2O_2$ $[M + H]^+$ 487.6651 revealed $[M + H]^+$ 487.6656.

2.1.3 (S)-N-(2-chloro-3-(trifluoromethyl)benzyl)-1-(2-fluoroethyl)-5-oxopyrrolidine-2-carboxamide (6)—Compound **6** (TZ5038) was prepared similarly to compound **4**. Compound **6** white solid (360 mg, 54% yield) was derived from compound **3** (600 mg, 1.8 mmol, 1.0 equiv.) and 1-bromo-2-fluoroethane (2.0 equiv.) ^{1}H NMR (400 MHz, $CDCl_3$): δ 7.64 (d, J = 8 Hz, 1H), 7.57 (d, J = 7.2 Hz, 1H), 7.34 (t, J = 7.6 Hz, 1H), 4.59 (d, J = 6 Hz, 2H), 4.39 – 4.53 (m, 1H), 4.19 – 4.24 (m, 1H), 3.74 – 3.90 (m, 1H), 3.14 – 3.29 (m, 1H), 2.43 – 2.56 (m, 1H), 2.26 – 2.37 (m, 2H), 1.97 – 2.06 (m, 1H); ^{13}C NMR (100 MHz, $CDCl_3$): δ 176.0, 171.4, 137.6, 133.6, 131.6, 129.1 (q, J_{C-F} = 30.8 Hz), 127.1 (q, J_{C-F} = 5.4 Hz), 126.9, 122.7 (q, J_{C-F} = 272 Hz), 82.8 (d, J_{C-F} = 166.7 Hz), 62.3 (d, J_{C-F} = 2.1 Hz), 42.5 (d, J_{C-F} = 19.4 Hz), 41.7, 29.3, 28.8. HRMS (ESI) calculated for $C_{15}H_{15}ClF_4N_2O_2$ $[M + H]^+$ 367.0831 revealed $[M + H]^+$ 367.0836.

2.2 Radiochemistry

The radiosynthesis of [^{123}I]TZ6019 was depicted in Scheme 1B. Briefly, 111 MBq [^{123}I]NaI (Nordion International Inc., Ottawa, Canada) was added to a mixture of tin-precursor **4** (300 to 400 μg) in 30 μl acetonitrile (ACN) and 50 μl of a 5% (w/v) solution of sodium acetate in glacial acetic acid, followed by the addition of 50 μl of an oxidant solution consisting of a 2:l ratio (v/v) of acetic acid/H_2O_2 (30%). After the mixture was stirred at room temperature for 15 min, the residue was injected into a reversed-phase semi-preparative high-performance liquid chromatography (HPLC) column (250×9.6 mm, 5 μm) equipped with a 1 ml injection loop for purification. The system was operated at a flow rate of 2 ml/min with ACN/0.1M ammonium formate (AMF) (50/50, v/v, pH = 4.5) as the mobile phase. The retention times of free iodine and the desired product were 4 and 17 min, respectively. Under these conditions, product was collected in a flask containing sterile water (50 ml). The diluted aqueous solution was passed through C18 Sep-Pak Plus (WAT020515, Waters, Milford, MA), and washed with water (20 ml). Final radioactive product [^{123}I]TZ6019 was eluted using EtOH (0.6 ml).

2.3 Radioligand binding assay

2.3.1 HEK-293-hP2X7 receptor cell culture—HEK-293 cells stably transfected with the human P2X7 receptor (HEK-293-hP2X7R) were maintained in Dulbecco's Modified Eagle's Medium (DMEM) supplemented with 10% fetal calf serum, antibiotics (50 Units/ml

penicillin and 50 μg/ml streptomycin) and 300 μg/mL Geneticin (Invitrogen Inc., Carlsbad, CA). Cells were grown in a 75 ml cell culture flask with a humidified atmosphere of 5% CO_2 at 37 °C. Confluent HEK293-hP2X7R cells were washed twice with cold PBS, then FACS (Fluorescence Activation Cell Sorting) and western blot experiments confirmed expression of P2X7 receptor were followed as our previous publication (Han et al., 2017).

2.3.2 *In vitro* fluorescence assay for measurement uptake of ethidium bromide —Activation of P2X7 receptor-associated pore formation was observed using a fluorescence plate reader by measuring the cellular uptake of ethidium bromide dye in HEK-293-P2X7R cells, as reported (Chessell et al., 1997; Michel et al., 2006; Park et al., 2016). For the actual assay, ~2×10^5 human HEK293-hP2X7R cells per well were placed in 96-well poly-lysine coated black microplate (Corning Inc., Kennebunk, ME) overnight. The phosphate-buffered saline (PBS) consisting of 137 mM NaCl, 2.7 mM KCl, 10 mM Na_2HPO_4, and 2 mM KH_2PO_4 was used for washing HEK293-P2X7 cells in the growth medium and was removed before performing the assay. Each well then was replaced with 90 μL of assay solution consisting of 4-(2-hydroxyethyl)-1-piperazineethanesulfonic acid (HEPES) (10 mM), *N*-methyl-D-glucamine (5 mM), KCl (5.6 mM), D-glucose (10 mM), and $CaCl_2$ (0.5 mM) (pH 7.4) and supplemented with 280 mM sucrose. Ten μl of 60 μM BzATP (final 6 μM), and of 10 μl of 10 × of the synthesized compound at serial diluted concentration (final concentration 0.3 nM – 3 μM) was added to each well. After incubation for 15 min, ethidium bromide uptake was detected by measuring the fluorescence with a VictoR3 plate reader (Perkin Elmer Inc., Waltham, MA), using an excitation wavelength of 540 nm and emission wavelength of 615 nm. The results were expressed as relative to the maximum accumulation of ethidium bromide when stimulated with BzATP only, and the IC_{50} values were determined using nonlinear regression by 3-parameter inhibitor-effect equation in Prism (GraphPad Software, Inc., San Diego, CA).

2.3.3 Radioligand saturation binding assay—For saturation binding studies, ~2×10^5 human HEK293-hP2X7R cells per well were placed in regular 96-well poly-lysine coated microplate (Bioworld Inc., Dublin, OH) overnight. Culture medium was removed on the second day, and cells were washed three times with 250 μl/well ice-cold assay buffer that was 50 mM Tris–HCl pH 7.4 with 0.1% BSA. Then 90 μl/well of assay buffer with serial diluted [^{123}I]TZ6019, and 10 μl of assay buffer only (for total binding) or 10 μl of assay buffer with 100 μM final concentration of cold GSK1482160 were added (for nonspecific binding). The final concentration of [^{123}I]TZ6019 ranged from 0.2 – 400 nM, calculated based on the stock radioactivity concentration and the theoretic specific activity (34.7 GBq/μmol). Triplicate wells were made for each concentration in the assay. Wells were incubated for 1 h on ice in a shaking water bath. Binding activities were terminated by rapid washing of the plate 5 times with 200 μl/well of ice-cold assay buffer. After the last wash, 100 μl/well of 0.5% sodium dodecyl sulfate (SDS) was added. After 1–2 min clean cell lysate from the 96-well microplate were transferred to a scintillation 96-well microplate (PerkinElmer Life and Analytical Sciences Inc., Shelton, CT), and 200 μl of Bio-Safe II complete counting cocktail (RPI research products Inc., Mount Prospect, IL) were added to each sample. Radioactivity of each sample was counted on a Wallac 1450 MicroBeta TriLux liquid scintillation counter (PerkinElmer, Boston, MA). Each sample was counted 30 s at the

energy window of 5–1024 kev, and radioactivity of all samples (cpm) were decay corrected (half-life of 13.3 h) to the time when the first well was counted. Data analysis was accomplished using GraphPad Prism (GraphPad Software, Inc., San Diego, CA). The specifically bound counts (cpm) from the saturation binding experiments were calculated by subtracting the non-specific binding from the total binding. The binding assay data were curve-fit to a one-site binding (hyperbola) equation to derive the dissociation constant of the radioligand (K_d) and number of binding sites (B_{max}, fmol/ mg), in which the cpm and cell number were normalized to fmol/mg as described for the online internal Prism calibration procedures: http://www.graphpad.com/quickcalcs/radcalch).

2.3.4 Radioligand competition binding assay using [^{123}I]TZ6019—In radioligand competition binding studies, ~2 × 10^5 HEK293-hP2X7R cells were placed in 96-well poly-lysine coated microplate (Bioworld Inc., Dublin, OH) overnight. Culture medium was removed on the second day, and cells were washed three times with 250 μl/well ice-cold assay buffer (50 mM Tris–HCl pH 7.4 with 0.1% BSA). Then 80 μl/well of assay buffer, 10 μl of assay buffer with serial diluted cold GSK1482160 or TZ6019, final concentration in the range of 0.1 nM – 3 μM), and 10 μl of assay buffer with fixed concentration of [^{123}I]TZ6019 (final 9.7 nM) were added. Wells without adding the testing compound were considered as the maximum bound, and wells adding 100 μM of GSK1482160 were considered as the non-specific bound. Triplicate wells were made for each concentration in the assay. The rest of the procedure was as same as the saturation binding. The specific bound counts (the nonspecific bound counts subtracted from the total observed counts) (cpm) were expressed as a percentage of the maximal bound, and then these binding data were curve-fit to a 3-parameter inhibitor-effect equation to derive the potency (IC_{50}) of the test compound in Prism (GraphPad Software, Inc, San Diego, CA). The equilibrium dissociation constant (K_i) of the test compound was calculated by the Cheng–Prusoff equation (Cheng and Prusoff, 1973): $K_i = IC_{50}/(1 + L^*/K_d)$, Where L* is the [^{123}I]TZ6019 concentration used and K_d was set to the mean value from saturation binding assays.

2.3.5 Radioligand competition binding assay using [^{3}H]A804598—Radioligand [^{3}H]A804598 was purchased from Moravek Inc. (Brea, CA USA). For all experiments, ~2×10^5 HEK293-hP2X7R cells were placed in 96-well poly-lysine coated microplate (Bioworld Inc., Dublin, OH) overnight. Followed the same procedure as the [^{123}I]TZ6019 based radioligand competition assay. Nonspecific binding was determined in the presence of GSK1482160 (100 μM). All assays were carried out at 4°C incubations by the adding of 80 μl of assay buffer to the cell, 10 μl of assay buffer with fixed concentration of [^{3}H]A804598 (2 nM based on radioactivity concentration and specific activity 1.33 GBq/μmol), and 10 μl of assay buffer with serial diluted compounds including GSK1482160 and TZ6019. The final concentration ranged from 0.1 nM – 3 μM. The binding–effect data were curve-fit to a 3-parameter inhibitor-effect equation to derive the potency (IC_{50}) of the test compound using Prism (GraphPad Software, Inc., San Diego, CA).

2.4 Mutant tau P301S mouse model

All rodent experiments were conducted in compliance with the Guidelines for the Care and Use of Research Animals under protocols approved by Washington University's Animal

Studies Committee. P301S transgenic mice expressing the human tau P301S mutant form of human microtubule-associated protein tau (MAPT) under the direction of the mouse prion protein promoter (Prnp) and resulting in 5-fold greater human tau expression over endogenous mouse tau protein (Yoshiyama et al., 2007). Breeding pairs were purchased from the Jackson Laboratory, and resulting progenies were maintained on a B6C3 background to generate both P301S transgenic and wild type littermate controls. Mice had access to food and water *ad libitum* and were housed on a 12-hour light/dark cycle. Nine-month-old P301S mutant mice, along with their wild type littermates, were applied for this study.

2.5 *In vitro* autoradiography studies of P301S mouse brain

After saline perfusion and euthanasia of the mice, brain tissue was quickly collected and each mouse brain was cut sagittal into two parts along the midline. One half-brain was directly frozen in liquid nitrogen for post-mortem autoradiography studies; the other half was drop-fixed in 4% formaldehyde at 4°C for use in immunofluorescence microscopy studies. For autoradiography studies, 20 μm slices from P301S mice and wild type control mice were incubated with 2.8 MBq/mL [^{123}I]TZ6019 on ice for 60 min, following by a 15-min pre-incubation in assay buffer (50 mM Tris–HCl buffer, pH 7.4, 0.1% BSA, and 1 mM EDTA). Following this incubation, sections were washed 2 times in assay buffer at 4 °C and rinsed once using distilled water at 4°C to remove buffer salts. Then the slides were air-dried and exposed to the storage phosphor screen (Fuji Photo Film Inc., Tokyo, Japan) in an imaging cassette for 2 – 4 hr in 4°C at dark. The distribution of radioactivity was visualized by a Fuji Bio-Imaging Analyzer FLA-7000 (GE healthcare Life Sciences Inc., Pittsburgh, PA). Photo-stimulated luminescence was quantified in one representative brain section using Multi Gauge v3.0 software (Fuji Photo Film Inc., Tokyo, Japan). Data were background-corrected and expressed as photo-stimulated luminescence signals per square millimeter (PSL/mm^2). For statistical comparison, the student t-test were applied using MS Excel and $p < 0.05$ was considered statistically significant.

2.6 Immunofluorescence (IF) microscopy

The fixed brain tissue was cut into 50 μm slices, stored free-floating in cryoprotectant solution (10% ethylene glycol, 30 mM phosphate buffer, 15% sucrose) and kept at 4°C until use. Slices were blocked at room temperature for 1 h in 5% normal horse serum (NHS) prior to incubation with the primary antibodies: P2X7 receptor (rabbit anti-P2X7 receptor polyclonal antibody, 1:50, Alomone labs Inc., Jerusalem, Israel), and GFAP (chicken anti-GFAP polyclonal antibody, 1:1000, Abcam Inc, Cambridge, MA) in 5% NHS with 1× TBS 0.1% Triton X-100 overnight at 4°C. Sections were incubated for 1 h at room temperature with fluorescent-conjugated secondary antibodies (1:1000 anti-chicken DyLight 488 and 1:1000 anti-rabbit Alex 594, ThermoFisher Scientific Inc., Waltham, MA) and counter stained with DAPI for 5 min. Sections were then mounted onto slides, and cover slipped using Fluoromount G mounting solution (Southern Biotech Inc., Birmingham, AL). The 60× confocal microscope images were collected from a Nikon A1Rsi scanning confocal microscope system in the Washington University Center for Cellular Imaging. All images were taken with the same fluorescent settings and subsequently adjusted equally for brightness and contrast to ensure accurate pathologic quantification.

3. Results

3.1 Chemistry

The precursor desmethyl-GSK1482160 was synthesized by following standard methods (Gao et al., 2015; Han et al., 2017) (Scheme 1A). The condensation of L-pyroglutamic acid with amine under 1-ethyl-3-(3-dimethylaminopropyl) carbodiimide hydrochloride (EDAC) and 1-hydrobenzotrizole (HOBt) produced product **3** in 70% yield. Then reaction of desmethyl-GSK1482160 **3** with tributyl-(3-chloro-propenyl)-stannane in the presence of LiHMDS gave the radiolabeling precursor **4**. Iodination of precursor in chloroform afforded the standard reference **5** (TZ6019) in good yield (65%). The fluoroethyl modified compound **6** (TZ5038) was produced from **3** and 1-bromo-2-fluoroethane in similar procedure. The structure of compound **4, 5, 6** were confirmed by NMR spectroscopy and LC-MS.

3.2 Radiochemistry

The one-step iodine-123 radiolabeling of the tin precursor **4** proceeded smoothly at room temperature. Under the optimized conditions (Scheme 1B), the product was obtained in high yield (85 ± 5%, n = 8, decay corrected to the end of synthesis), excellent radiochemical purity (> 99%), and theoretical specific activity 34 GBq/μmol.

3.3 Fluorescence assay

A fluorescence assay based on the ethidium bromide measurement of the pore permeation was used to assess the binding potency of the newly synthesized iodinated compounds and other known P2X7 compounds. The known P2X7 compound GSK1482160 used as an internal control had an IC_{50} value of 2.10 ± 0.30 nM, consistent with previous reports (Gao et al., 2015; Han et al., 2017). The fluoroethyl modified compound **6**, TZ5038 (9.93 ± 2.1 nM) showed slightly higher IC_{50} value compared to GSK1482160 (Fig. 2, Table 1). The assay revealed that iodinated compounds TZ6019 had 5-fold (9.75 ± 1.2 vs 2.10 ± 0.3 nM) lower binding potency than compound GSK1482160 (Scheme 1, Table 1), but similar binding potency to the fluoroethyl substituted compound TZ5038, suggesting that extending the alkyl chain of pyrrolidine may interfere with the P2X7 receptor binding but the binding potency was still in nanomolar range.

3.4 Saturation binding [^{123}I]TZ6019

At the radioligand saturating binding assays, non-specific binding of [^{123}I]TZ6019 remained constant in 2–5×10^5 cells of HEK-hP2X7R, suggesting that the non-specific binding to the cell is minimal (Fig.3.). The specific binding curve showed a typical saturation binding curve, with nanomolar range (K_d = 19.3 ± 2.8 nM) of binding affinity (Fig. 3). The low dissociation rate permits the washing of the plate for the separation of free from bound radioligand (Han et al., 2017; Letavic et al., 2013; Territo et al., 2016), while the association rate supports 60 min incubations for attaining steady-state binding. The saturation binding data indicated that specific binding represented approximately 40% of total binding. The [^{123}I]TZ6019-based competition binding assay revealed that the IC_{50} value is 9.75 ± 1.2 nM and the calculated K_i value based on Cheng–Prusoff equation was 6.30 ± 0.9 nM. Therefore [^{123}I]TZ6019 binds to the recombinant human P2X7 receptor with high affinity. These

results were consistent with our fluorescence ethidium bromide assay result. The specific binding data fit a straight line on a Scatchard plot, indicating that one-site binding model is a good model for [^{123}I]TZ6019 binding to human P2X7 receptor. Receptor density (B_{max}) as determined by saturation binding with [^{123}I]TZ6019 was 262 ±10 fmol/mg, which were consistent with the carbon-11 labeled GSK1482160 measurement from previous studies (Han et al., 2017; Territo et al., 2016).

3.5 Competition binding potency

To validate the suitability of using radioligand [^{123}I]TZ6019 to screen P2X7 compounds, the competition binding assays applying radioligands [^{123}I]TZ6019 and [^{3}H]A804598 were carried out (Fig 2C, 2D, Fig 3A, 3B) and compared. The known P2X7 compound (GSK1482160) showed stronger binding (IC_{50} value of 4.3 ± 0.9 nM) in the [^{123}I]TZ6019 based radioactive competitive assay, while the values were 8.65 ± 1.0 nM using [^{3}H]A804598. The iodinated substituted analog TZ6019 (compound **5**), and fluoroethane substituted analog TZ5038 (compound **6**) showed similar trends in stronger binding in [I^{123}]TZ6019 based radioactive competitive assay (Table 1). Among these assays, radioactive competitive assay based [^{123}I]TZ6019 showed systematic stronger binding than using [^{3}H]A804598 (Table 1). The radioactive competitive assay results using [^{123}I]TZ6019 showed results consistent with the fluorescence assay.

3.6 *In vitro* autoradiography of [^{123}I]TZ6019 in brain tissue of P301S mice

To further evaluate the iodinated radioligand [^{123}I]TZ6019, *in vitro* autoradiography studies of [^{123}I]TZ6019 were performed to detect the expression of P2X7 receptor in the brain of a mouse model of tauopathy. P2X7 receptor expression was quantified using [^{123}I]TZ6019 was significantly elevated in P301S mice (Fig. 4, Table 2). Different brain regions including cortex, hippocampus, thalamus and total brain were quantified and compared to wild type (Fig. 5, Table 2). In hippocampus, P2X7 receptor was highly expressed in the P301S mice (n = 3, 255.05 ± 10.90 PSL/mm^2), which was 1.7-fold higher than the wild type mice group (154.18 ± 16.14 PSL/mm^2, n = 3, P = 0.00043). Specific binding in cortex (n = 3) was 330.53 ± 91.08 PSL/mm^2 for P301S mice which was 2.4-fold higher than in wild type mice (135.23 ± 32.55 PSL/mm^2; P = 0.012) (Fig. 4, 5, Table 2). The expression of P2X7 receptor in thalamus was also significantly higher in P301S mice than wild type mice (P = 0.039, n =3), 337.98 ± 93.45 PSL/mm^2 for P301S and 187.41 ± 61.02 PSL/mm^2. Finally the expression of P2X7 receptor in total brain was significantly higher in P301S mice than wild type mice (P = 0.043, n = 3), 260.86 ± 48.93 PSL/mm2 for P301S and 193.05 ± 39.92 PSL/mm2. An overall increasing trend (P = 0.0013) was found when including all regions quantified.

3.7 Expression of P2X7 receptor and astrocytes staining in P301S mice

Immunofluorescence (IF) staining was done in the other half of the brain tissues from P301S and wild type mice. The data revealed that astrocytes (GFAP, green) colocalized with P2X7 receptor (red) in the hippocampal region as visualized by the dual labeled yellow cells (Fig. 6). Overall, our IF microscopy results confirmed that expression of P2X7 receptor was up-regulated in brains of P301S mice, and colocalized with astrocytes.

4. Discussion

A number of radiolabeled P2X7 ligands have been reported (Donnelly-Roberts et al., 2009; Han et al., 2017; Honore et al., 2006; Janssen et al., 2014; Lord et al., 2015; Ory et al., 2016; Territo et al., 2016) (Fig. 1), but none of them have been successfully translated to human studies. Two tritiated radioligand [^{3}H]A804598 and [^{3}H]JNJ54232334, have been characterized in rat brain membranes (Donnelly-Roberts et al., 2009; Lord et al., 2015). However, nonspecific binding may compromise the accurate analysis of P2X7 receptor binding with these radioligands (Lord et al., 2015). An analogue of GSK1482160 was originally discovered from GlaxoSmithKline with a high throughput screening for P2X7 receptor specific antagonists (Abdi et al., 2010; Chambers et al., 2010). Continuing the work on a C-11 labeled analogue, we synthesized and characterized the iodinated analogue TZ6019 in this study. We observed that the binding potency of TZ6019 was in nanomolar range. We applied both [^{123}I]TZ6019 and [^{3}H]A804598 to screen compounds by the radioligand competitive assay, slightly lower IC_{50} values were observed using [^{123}I]TZ6019 compared to [^{3}H]A804598 (Table 1). A larger pool of compounds will need to be screened to confirm this relationship. Compounds that show significant differences in binding potency using these two different radioligands may provide valuable insight information for the P2X7 binding properties for different chemical classes, represented by TZ6019 vs A804598. Compared to the relatively higher non-specific binding of [^{3}H]804598 (Lord et al., 2015), [^{123}I]TZ6019 may provide higher specific binding to P2X7 receptor. In addition, the synthesis of [^{123}I]TZ6019 is easily achieved with significantly higher yields compared to [^{3}H]804598. [^{123}I]TZ6019 has advantages for use as a screening radioligand to determine the binding potency of compounds to P2X7 receptor.

Transgenic P301S mice display neuroinflammation with microglial activation and astrogliosis at 9 month old age (Lopez-Gonzalez et al., 2015). The ultrastructure of the neurofibrillay tangle-like lesions in these mice is similar to that found in brain lesions of human AD and tauopathy patients. In addition to the promising *in vitro* binding studies, we quantified the P2X7 receptor expression in brain of P301S mice by [^{123}I]TZ6019. The *in vitro* autoradiography revealed that [^{123}I]TZ6019 has significantly higher specific binding in P301S mice (Fig 4, 5). This suggests that [^{123}I]TZ6019 may be used to assess neruroinflammatory response in AD or tauopathy. Athough the expression of P2X7 receptor in brain regions was globally increased, the hippocampus, cortex, and thalamus regions were significantly increased (Tabel 2). The IF results further support that the P2X7 receptor elevation in hippocampus, associating with an increased expression of astrocytes in P301S mice (Fig. 6).

These results agree with previous report for astrocytic activation in P301S mice, but previous studies did not measure the P2X7 receptor expression (Lopez-Gonzalez et al., 2015). In mouse models of AD, astrocytes or microglia exhibit abnormal activation and produce pro-inflammatory mediators (Lopez-Gonzalez et al., 2015; Parvathenani et al., 2003). P2X7 receptor plays a vital role in astrocytes/microglia-mediated IL-1β processing and release through the membrane receptors, which promotes inflammatory damage in CNS (Grygorowicz et al., 2016; Jimenez-Pacheco et al., 2016). The elevated expression of P2X7 receptor in AD mice model of tg2576 mice was reported (Parvathenani et al., 2003), but the

expression of P2X7 receptor in a tauopathy model has not been reported. In this study, we characterized *in vitro* binding of [^{123}I]TZ6019 with brain tissue of P301S mice, a tauopathy mouse model. To the best of our knowledge, this is the first investigation of P2X7 receptor in the P301S mice.

P2X7 radioligands have demonstrated utility for *in vivo* imaging studies; the P2X7 radioligand [^{11}C]GSK1482160 as a PET radioligand has been reported recently (Han et al., 2017; Ory et al., 2016). Understanding the interaction of P2X7 receptor with its ligands is key to developing therapeutic strategies targeting this receptor. However the weak binding affinity to rodent P2X7 receptor may limit the application of this radiotracer (Gao et al., 2015; Han et al., 2017; Ory et al., 2016). Additional new radioligands are still needed in the future. Compared to compound GSK1482160, the fluoroethane or iodinated modification showed similar binding potency to P2X7 receptor with minor reduction of binding potency based on IC_{50} values. *In vivo* binding specificity is a key parameter for a novel radiotracer. Without using P2X7 receptor knockout mice to characterize the in vivo binding specificity of [^{123}I]TZ6019 was a limitation. Our future study of promising P2X7 receptor imaging radiotracers will use P2X7 receptor knockout mice to confirm their in vivo binding specificity. Nevertheless, the properties of [^{123}I]TZ6019 reported in current study, will facilitate the development of new selective P2X7 ligands for potential imaging and therapeutic applications.

5. Conclusion

A potent iodinated labeled radiotracer [^{123}I]TZ6019 for P2X7 receptor was successfully radiosynthesized and evaluated in this study. Our *in vitro* cell binding assays demonstrated that this radioligand specifically binds to recombinant human P2X7 receptor with nanomolar affinity. Our *in vitro* autoradiography revealed that [^{123}I]TZ6019 was able to detect the increase of P2X7 receptor expression in brain from P301S mutant transgenic mice. This compound represents a promising radioligand for screening new P2X7 compounds and assessing P2X7 receptor expression in neuroinflammatory related diseases.

Acknowledgments

This work was supported by USA Department of Energy (DOE)-Training in Techniques and Translation: Novel Nuclear Medicine Imaging Agents for Oncology and Neurology, DESC0008432, and Interdisciplinary Training in Translational Radiopharmaceutical Development and Nuclear Medicine Research for Oncologic, Neurologic, and Cardiovascular Imaging, DESC0012737, the Fixel Foundation, and USA National Institute of health/National Institute of Neurological Disorders and Stroke and National Institute on Aging (NIH/NINDS and NIA) NS075527, NIH/NINDS, NS103988 and NS103957, USA National Institute of health/National Institute of mental health (NIH/NIMH) MH092797.

Abbreviations

ACN	Acetonitrile
AD	Alzheimer’s disease
AMF	ammonium formate
ATP	adenosine-triphosphate

BzATP	3'-O-(4-Benzoyl)benzoyl ATP, strong agonist for P2X7 receptor
CNS	central nervous system
DMEM	Dulbecco's Modified Eagle's Medium
DMF	dimethylformamide
EDAC	1-ethyl-3-(3-dimethylaminopropyl) carbodiimide hydrochloride
EtOAc	ethyl acetate
ESI	electrospray ionization
GFAP	Glial fibrillary acidic protein
FACS	fluorescence activation cell sorting
HEK-293	human embryonic kidney cells 293
HEPES	4-(2-hydroxyethyl)-1-piperazineethanesulfonic acid
HOBt	1-hydrobenzotrizole
HPLC	high-performance liquid chromatography
HRMS	high resolution mass spectrum
hr	hour
IC_{50}	the concentration of an inhibitor where the response (or binding) is reduced by half
IF	Immunofluorescence
K_d	the equilibrium dissociation constant, inverse of association constant (Ka)
K_i	inhibition dissociation constant
LC-MS	liquid chromatography–mass spectrometry
LiHMDS	Lithium bis(trimethylsilyl)amide
MAPT	human microtubule-associated protein tau
NHS	normal horse serum
NMR	nuclear magnetic resonance
PBS	phosphate buffered saline
PD	Parkinson’s disease

PET	positron emission tomography
Prnp	prion protein promoter
PSL/mm^2	photo-stimulated luminescence signals per square millimeter
P2X7 receptor	P2X ligand-gated ion channel 7
ROI	region of interest
SDS	sodium dodecyl sulfate
TMS	tetramethylsilane
THF	tetrahydrofuran
TLC	Thin layer chromatography

References

Abdi MH, et al. Discovery and structure-activity relationships of a series of pyroglutamic acid amide antagonists of the P2X7 receptor. Bioorg Med Chem Lett. 2010; 20:5080–5084. [PubMed: 20673717]

Able SL, et al. Receptor localization, native tissue binding and ex vivo occupancy for centrally penetrant P2X7 antagonists in the rat. Br J Pharmacol. 2011; 162:405–414. [PubMed: 20840537]

Bartlett R, et al. The P2X7 receptor channel: recent developments and the use of P2X7 antagonists in models of disease. Pharmacol Rev. 2014; 66:638–675. [PubMed: 24928329]

Basso AM, et al. Behavioral profile of P2X7 receptor knockout mice in animal models of depression and anxiety: relevance for neuropsychiatric disorders. Behav Brain Res. 2009; 198:83–90. [PubMed: 18996151]

Bhattacharya A, Biber K. The microglial ATP-gated ion channel P2X7 as a CNS drug target. Glia. 2016; 64:1772–1787. [PubMed: 27219534]

Bhattacharya A, et al. Pharmacological characterization of a novel centrally permeable P2X7 receptor antagonist: JNJ-47965567. Br J Pharmacol. 2013; 170:624–640. [PubMed: 23889535]

Bianco F, et al. A role for P2X7 in microglial proliferation. J Neurochem. 2006; 99:745–758. [PubMed: 16836656]

Boumechache M, et al. Analysis of assembly and trafficking of native P2X4 and P2X7 receptor complexes in rodent immune cells. J Biol Chem. 2009; 284:13446–13454. [PubMed: 19304656]

Burnstock G. Purinergic cotransmission. Exp Physiol. 2009a; 94:20–24. [PubMed: 18723580]

Burnstock G. Purinergic signalling: past, present and future. Braz J Med Biol Res. 2009b; 42:3–8. [PubMed: 18853040]

Chambers LJ, et al. Synthesis and structure-activity relationships of a series of (1H-pyrazol-4-yl)acetamide antagonists of the P2X7 receptor. Bioorg Med Chem Lett. 2010; 20:3161–3164. [PubMed: 20399651]

Cheng Y, Prusoff WH. Relationship between the inhibition constant (K1) and the concentration of inhibitor which causes 50 per cent inhibition (I50) of an enzymatic reaction. Biochem Pharmacol. 1973; 22:3099–3108. [PubMed: 4202581]

Chessell IP, et al. Properties of the pore-forming P2X7 purinoceptor in mouse NTW8 microglial cells. Br J Pharmacol. 1997; 121:1429–1437. [PubMed: 9257924]

Collo G, et al. Tissue distribution of the P2X7 receptor. Neuropharmacology. 1997; 36:1277–1283. [PubMed: 9364482]

Donnelly-Roberts DL, et al. [^{3}H]A-804598 ([^{3}H]2-cyano-1-[(1S)-1-phenylethyl]-3-quinolin-5-ylguanidine) is a novel, potent, and selective antagonist radioligand for P2X7 receptors. Neuropharmacology. 2009; 56:223–229. [PubMed: 18602931]

Ferrari D, et al. The P2X7 receptor: a key player in IL-1 processing and release. J Immunol. 2006; 176:3877–3883. [PubMed: 16547218]

Franke H, Illes P. Pathological potential of astroglial purinergic receptors. Adv Neurobiol. 2014; 11:213–256. [PubMed: 25236731]

Gao M, et al. Synthesis of [(11)C]GSK1482160 as a new PET agent for targeting P2X(7) receptor. Bioorg Med Chem Lett. 2015; 25:1965–1970. [PubMed: 25819093]

Grygorowicz T, et al. Early P2X7R-related astrogliosis in autoimmune encephalomyelitis. Mol Cell Neurosci. 2016; 74:1–9. [PubMed: 26921791]

Han J, et al. Pharmacologic characterizations of a P2X7 receptor-specific radioligand, [^{11}C]GSK1482160 for neuroinflammatory response. Nucl Med Commun. 2017; 38:372–382. [PubMed: 28338530]

Honore P, et al. A-740003 [N-(1-{[(cyanoimino)(5-quinolinylamino) methyl]amino}-2,2-dimethylpropyl)-2-(3,4-dimethoxyphenyl)acetamide], a novel and selective P2X7 receptor antagonist, dose-dependently reduces neuropathic pain in the rat. J Pharmacol Exp Ther. 2006; 319:1376–1385. [PubMed: 16982702]

Janssen B, et al. Synthesis and initial preclinical evaluation of the P2X7 receptor antagonist [(1)(1)C]A-740003 as a novel tracer of neuroinflammation. J Labelled Comp Radiopharm. 2014; 57:509–516. [PubMed: 24995673]

Jimenez-Pacheco A, et al. Transient P2X7 Receptor Antagonism Produces Lasting Reductions in Spontaneous Seizures and Gliosis in Experimental Temporal Lobe Epilepsy. J Neurosci. 2016; 36:5920–5932. [PubMed: 27251615]

Letavic MA, et al. Synthesis and Pharmacological Characterization of Two Novel, Brain Penetrating P2X7 Antagonists. ACS Med Chem Lett. 2013; 4:419–422. [PubMed: 24900687]

Lopez-Gonzalez I, et al. Neuroinflammatory Gene Regulation, Mitochondrial Function, Oxidative Stress, and Brain Lipid Modifications With Disease Progression in Tau P301S Transgenic Mice as a Model of Frontotemporal Lobar Degeneration-Tau. J Neuropathol Exp Neurol. 2015; 74:975–999. [PubMed: 26360374]

Lord B, et al. A novel radioligand for the ATP-gated ion channel P2X7: [^{3}H] JNJ-54232334. Eur J Pharmacol. 2015; 765:551–559. [PubMed: 26386289]

Michel AD, et al. Decavanadate, a P2X receptor antagonist, and its use to study ligand interactions with P2X7 receptors. Eur J Pharmacol. 2006; 534:19–29. [PubMed: 16487507]

Monif M, et al. Microglia: proliferation and activation driven by the P2X7 receptor. Int J Biochem Cell Biol. 2010; 42:1753–1756. [PubMed: 20599520]

Monif M, et al. The P2X7 receptor drives microglial activation and proliferation: a trophic role for P2X7R pore. J Neurosci. 2009; 29:3781–3791. [PubMed: 19321774]

Ory D, et al. Preclinical Evaluation of a P2X7 Receptor-Selective Radiotracer: PET Studies in a Rat Model with Local Overexpression of the Human P2X7 Receptor and in Nonhuman Primates. J Nucl Med. 2016; 57:1436–1441. [PubMed: 27199364]

Park JH, et al. Potent Suppressive Effects of 1-Piperidinylimidazole Based Novel P2X7 Receptor Antagonists on Cancer Cell Migration and Invasion. J Med Chem. 2016; 59:7410–7430. [PubMed: 27427902]

Parvathenani LK, et al. P2X7 mediates superoxide production in primary microglia and is upregulated in a transgenic mouse model of Alzheimer's disease. J Biol Chem. 2003; 278:13309–13317. [PubMed: 12551918]

Territo PR, et al. Characterization of [^{11}C]-GSK1482160 for targeting the P2X7 receptor as a biomarker for neuroinflammation. J Nucl Med. 2016; 58:458–465. [PubMed: 27765863]

Yoshiyama Y, et al. Synapse loss and microglial activation precede tangles in a P301S tauopathy mouse model. Neuron. 2007; 53:337–351. [PubMed: 17270732]

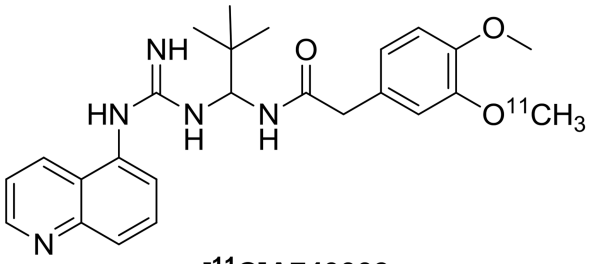

[^{11}C]A740003

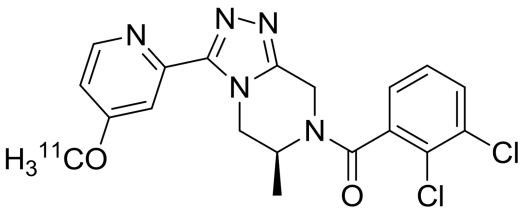

[^{11}C]JNJ54173717

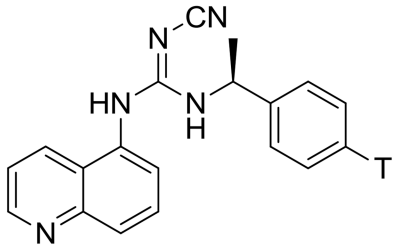

[^{3}H]A804598

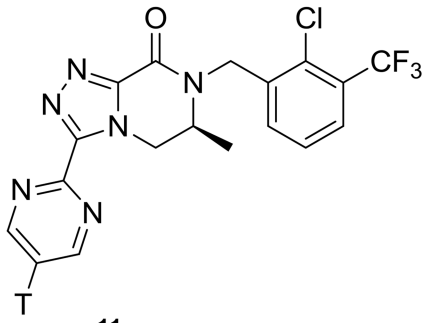

[^{11}C]JNJ54232334

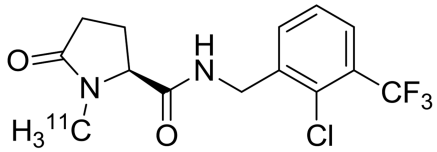

[^{11}C]GSK1482160

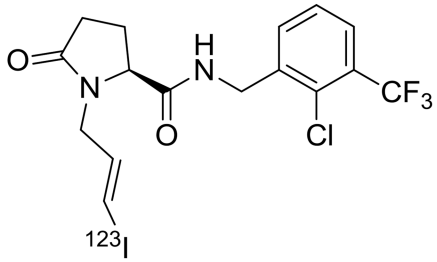

[^{123}I]TZ6019

Fig. 1.
Chemical structures of radioligands for P2X7 receptor.

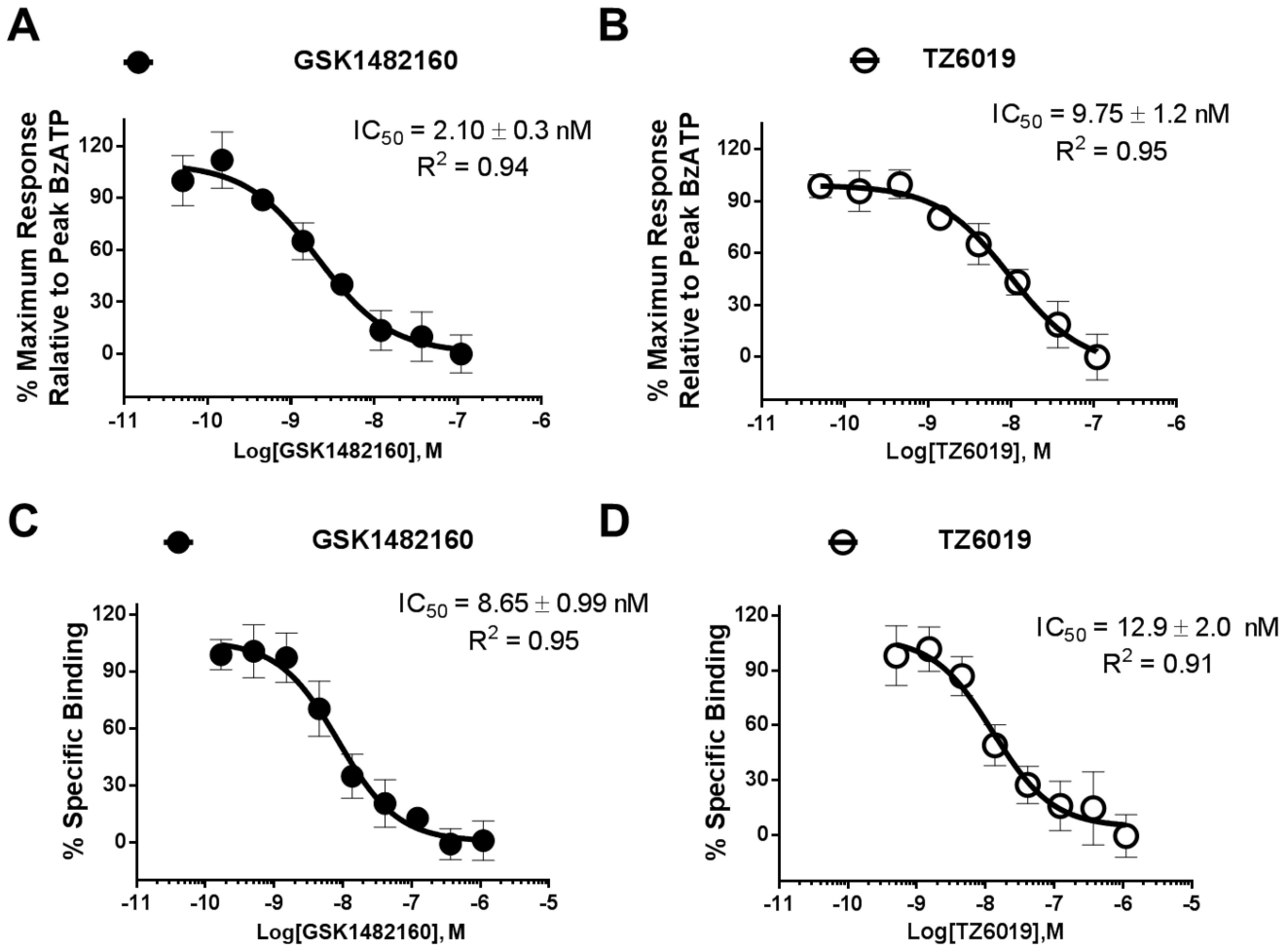

Fig. 2.

Characterization of compound TZ6019 binding to HEK-293 cells expressed recombinant human P2X7 receptor. Representative binding curves from fluorescence assay for GSK1482160 (filled circles) (A) and TZ6019 (open circles) (B), and from [^{3}H]A804598 based radioactive competitive binding curve for GSK1482160 (filled circles) (C) and TZ6019 (open circles) (D). The reported IC_{50} values (nM) were based on three independent assays with mean ± S.D..

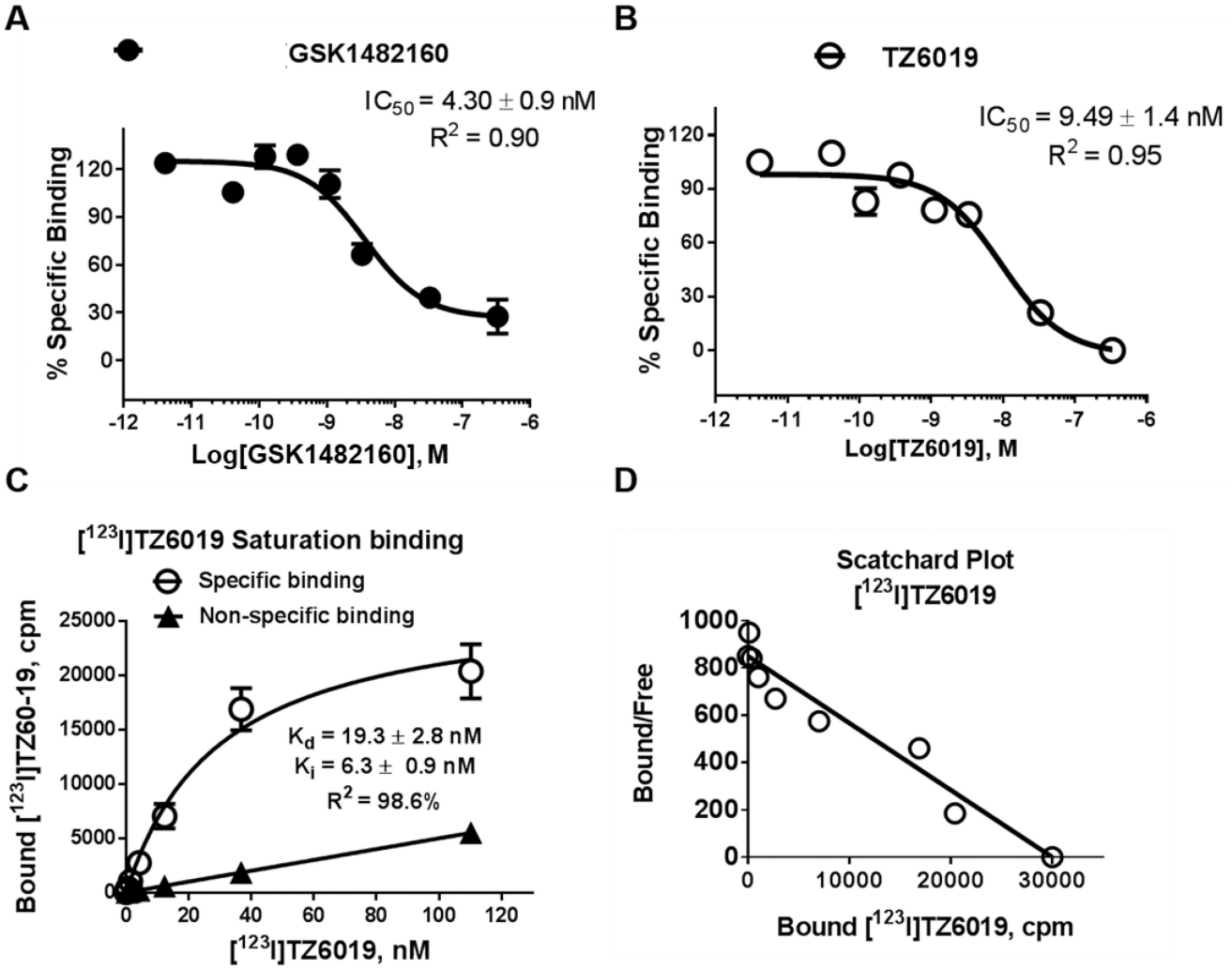

Fig. 3.

Characterization of [^{123}I]TZ6019 binding to HEK-293 cells expressed recombinant human P2X7 receptor. [^{123}I]TZ6019 based radioligand competitive binding curve for GSK1482160 (A) and TZ6019 (B). C. Saturation binding curve in the range of 0.2 – 115 nM of [^{123}I]TZ6019. The curve fitted K_d is 19.3 ± 2.8 nM (n = 3) and B_{max} is 262 fmol/mg (n = 3). The calculated K_i is 6.3 ± 0.9 nM (n = 3) based on Cheng-Prusoff equation. The reported IC50 or K_d values (nM) were based on three independent assays with mean ± S.D.. D. The specific binding data is fitted a straight line in Scatchard plot.

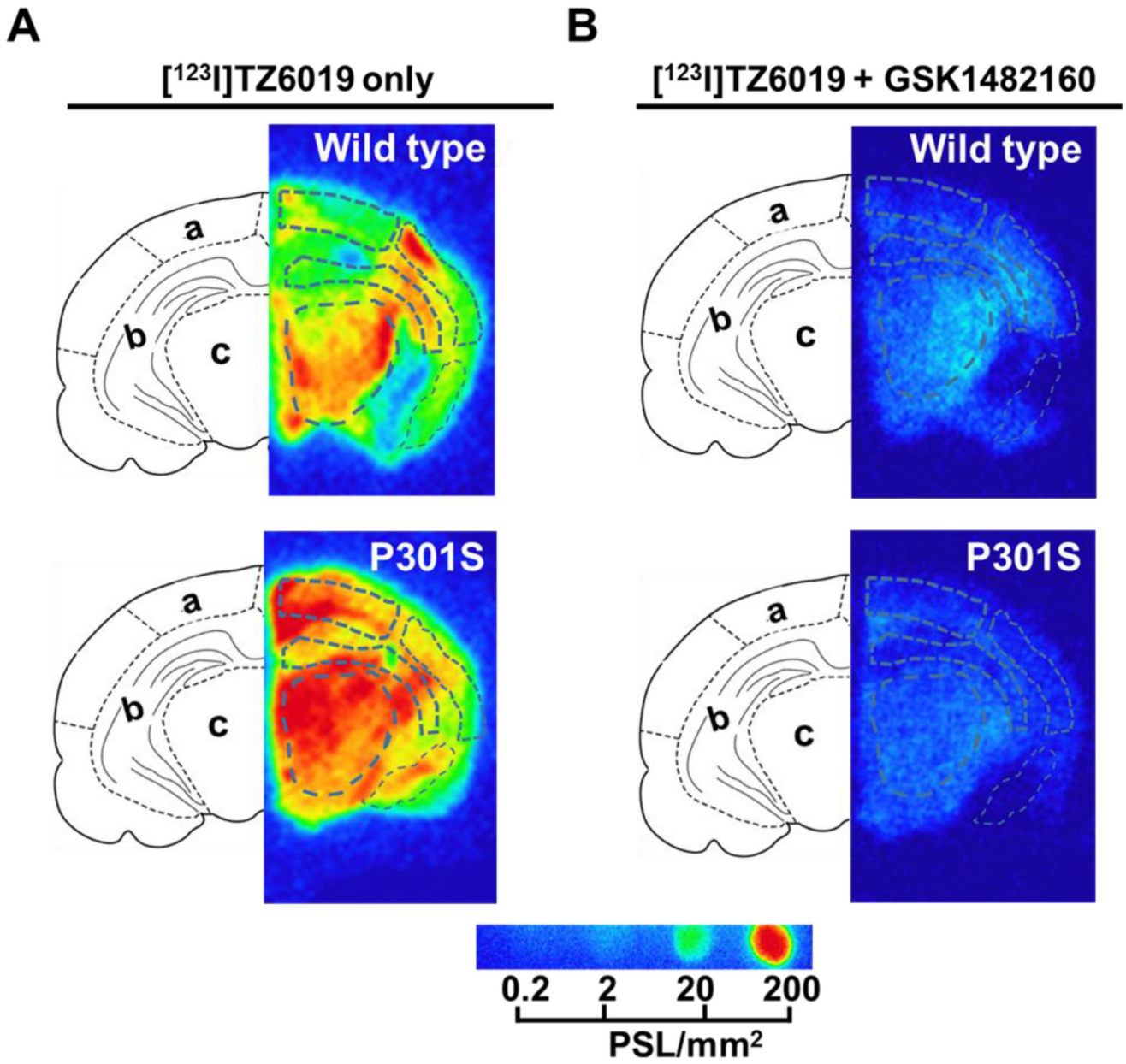

Fig. 4.

In vitro autoradiography of [^{123}I]TZ6019 for P301S mice and wild type control. The 20 μm coronal ipsilateral slices from P301S tau transgenic and healthy wild type mice, were incubated with [^{123}I]TZ6019 alone (A) or [^{123}I]TZ6019 plus 100 μM cold GSK1482160 (B) at room temperature for 60 min. Brain region keys: (a) Cortex, (b) Hippocampus, and (c) Thalamus.

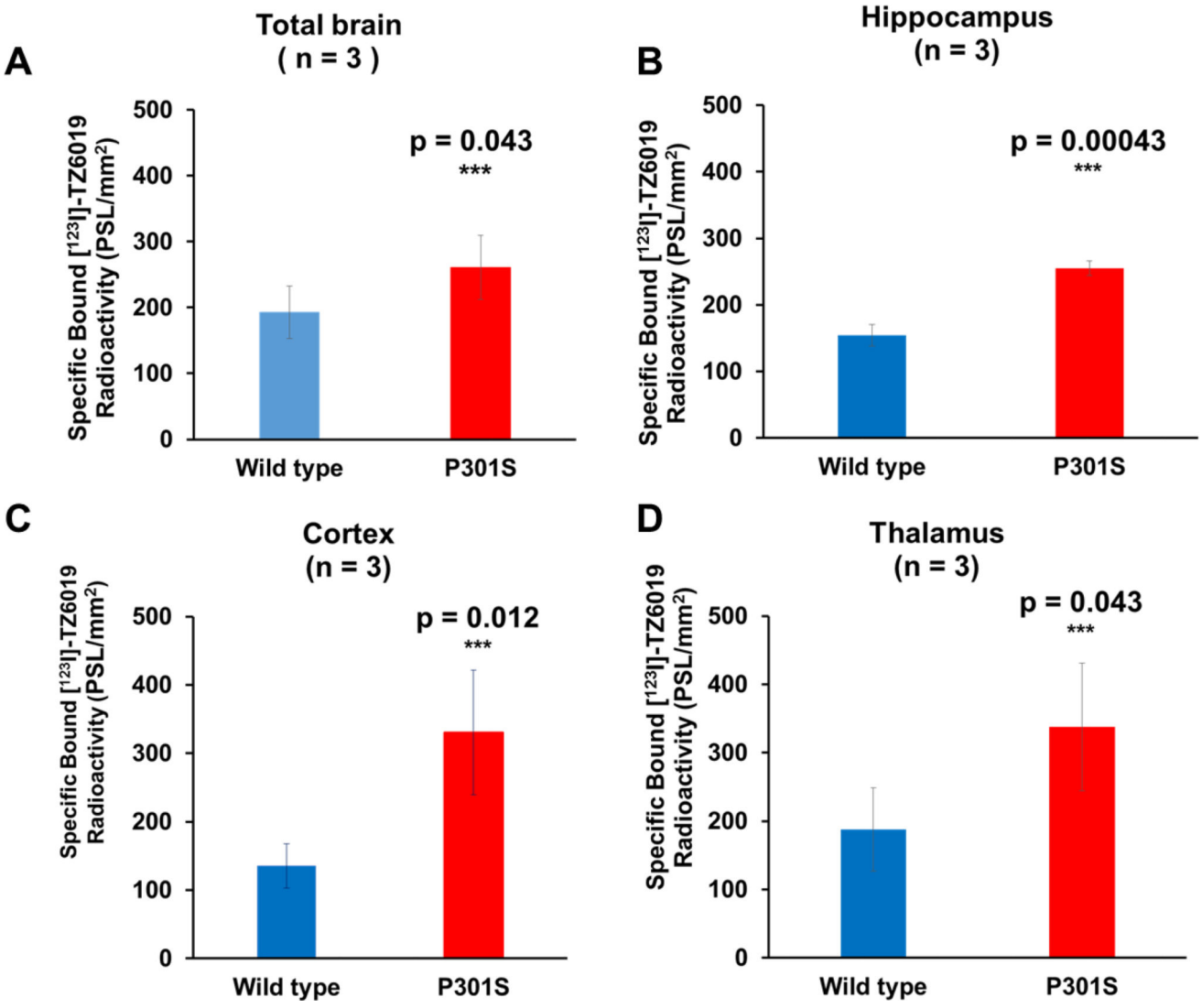

Fig. 5.

Elevation of P2X7 receptor expression in P301S mice was quantified *in vitro* autoradiography by [^{123}I]TZ6019. Quantitative histogram of higher binding of [^{123}I]TZ6019 in total brain (A), hippocampus (B), cortex (C), and thalamus (D) for P301S than wild type mice (n = 3, *** indicated student test $P < 0.05$). PSL/mm^2, photo-stimulated luminescence signals per square millimeter.

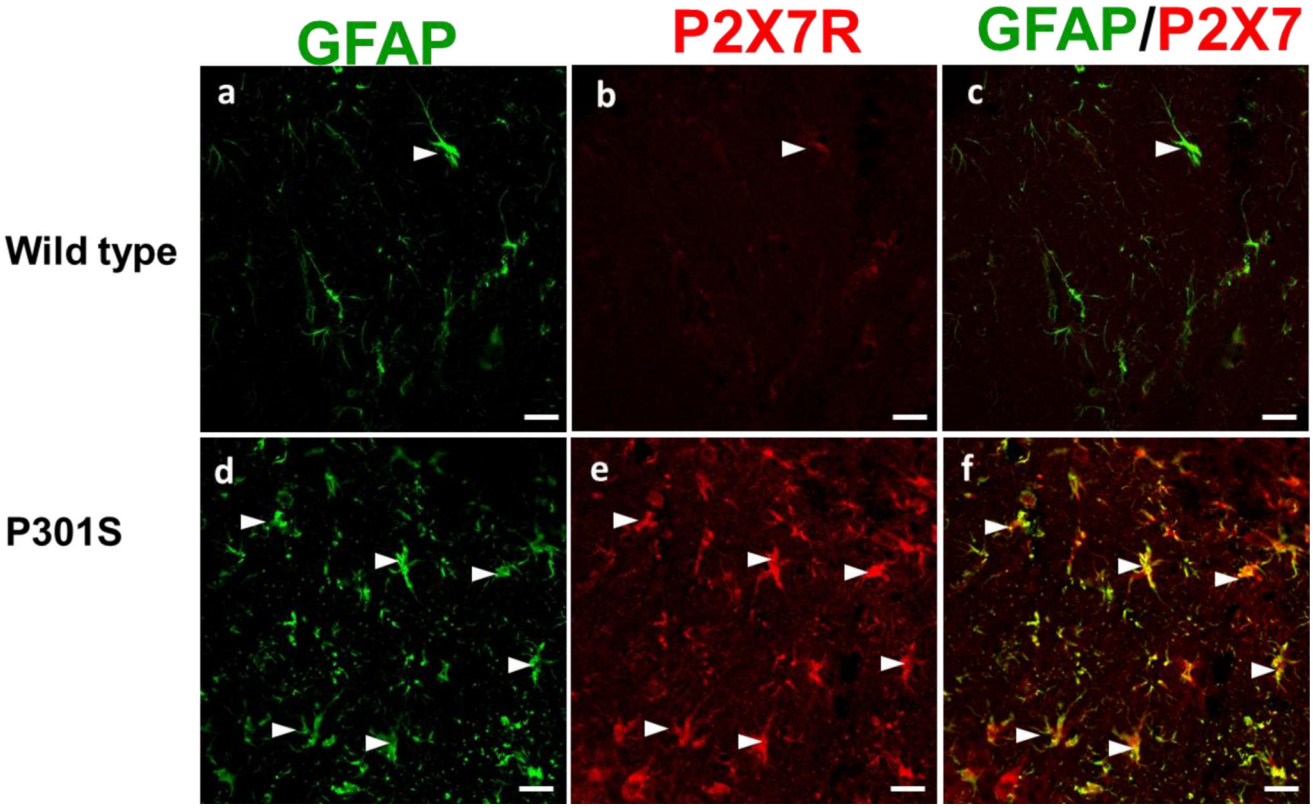

Fig. 6.

Immunofluorescence (IF) staining of elevation of P2X7 receptor and astrocyte activation in P301S mice. Representative IF confocal images demonstrate astrocytes expression (GFAP, green) in hippocampus of P301S mice (d, f), compared to wild type control mice (a, c). Representative IF images demonstrate elevation of P2X7 receptor (red) expression in brain of P301S mice (e), compared to wild type control mice (c). The colocalized astrocytes (green) and P2X7 receptor (red) in hippocampus region are depicted with white arrows. The white scale bar is 20 μm.

A. Synthesis

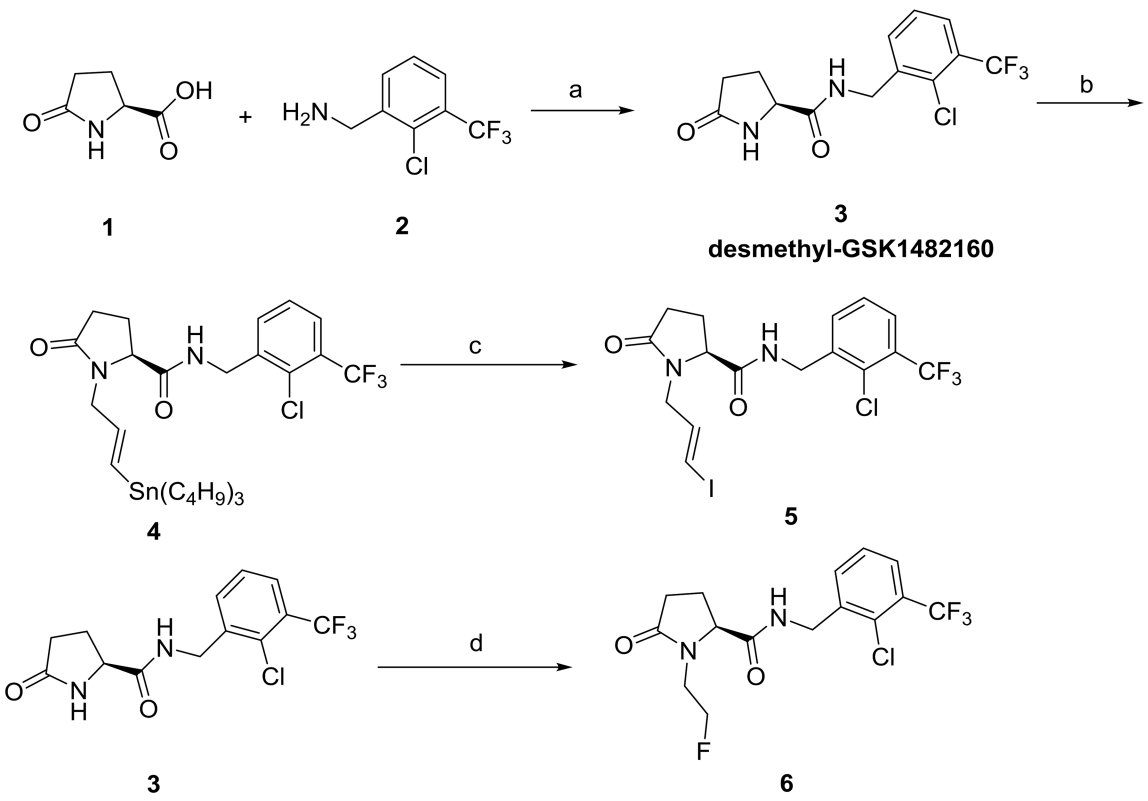

[a]Reagents and conditions: (a) 1-ethyl-3-(3-dimethylaminopropyl)carbodiimide hydrochloride, HOBt, DCM, rt; (b) tributyl-(3-chloro-propenyl)-stannane, LiHMDS, DMF; (c) I_2, $CHCl_3$, rt; (d) 1-bromo-2-fluoroethane, LiHMDS, DMF.

B. Radiosynthesis

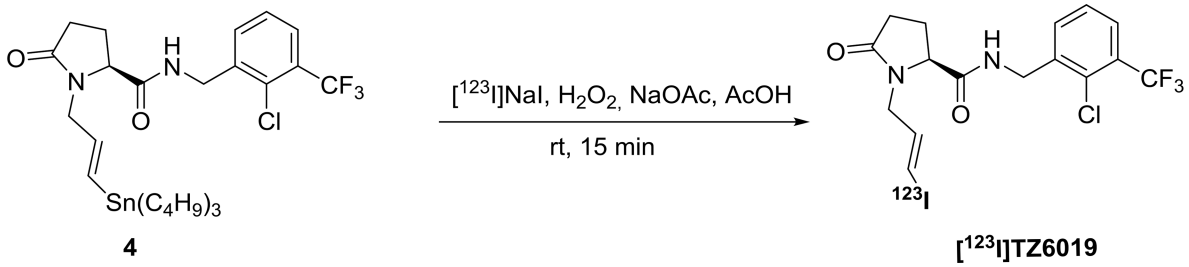

Scheme 1.

Synthesis of target compounds 5, 6 and radiolabeling of [^{123}I]TZ6019

[a]Reagents and conditions: (a) 1-ethyl-3-(3-dimethylaminopropyl)carbodiimide hydrochloride, HOBt, DCM, rt; (b) tributyl-(3-chloro-propenyl)-stannane, LiHMDS, DMF; (c) I_2, $CHCl_3$, rt; (d) 1-bromo-2-fluoroethane, LiHMDS, DMF.

Table 1

Summary of the P2X7 receptor binding potency (IC_{50} (nM), mean± S.D., n = 3) for 3 ligands obtained from different assays using HEK-293 transfected P2X7 receptor cells.

Compounds	Ethidium bromide Fluorescence assay IC_{50} (nM)	[^{123}I]TZ6019 Competition assay IC_{50} (nM)	[^{3}H]A804598 Competition assay IC_{50} (nM)
GSK1482160	2.10 ± 0.3	4.30 ± 0.9	8.65 ± 1.0
TZ6019 (compound 5)	9.75 ± 1.2	9.49 ± 1.4	12.9 ± 2.0
TZ5038 (compound 6)	9.93 ± 2.1	8.10 ± 1.3	11.90 ± 2.2

Table 2

Summary of P2X7 receptor expression quantified from the *in vitro* autoradiography in P301S and wild type mouse brain using [123I]TZ6019

ROI	P2X7 receptor expression quantified by autoradiography (PSL/mm^2, mean± S.D., n = 3)		P-value (t-test)
	Wild type	P301S	
Hippocampus	154.18 ± 16.14	255.05 ± 10.90	0.00043[a]
Cortex	135.23 ± 32.55	330.53 ± 91.08	0.012[a]
Thalamus	187.41 ± 61.02	337.98 ± 93.45	0.039[a]
Total brain	193.05 ± 39.92	260.86 ± 48.93	0.043[a]

[a] $P < 0.05$